Int J Earth Sci (Geol Rundsch) (2017) 106:1943–1961
DOI 10.1007/s00531-016-1399-8

ORIGINAL PAPER

Two-stage evolution of the Cenozoic Kunbei fault system and its control of deposition in the SW Qaidam Basin, China

Wen Zhu[1] · Chaodong Wu[1,2] · Jialin Wang[1] · Ya'nan Fang[1] · Chuanwu Wang[3] · Qilin Chen[4] · Huaqing Liu[4]

Received: 26 December 2015 / Accepted: 5 September 2016 / Published online: 24 September 2016

Abstract The structural relationship between the Qaidam Basin and Qimen Tagh-Eastern Kunlun Range holds important implications for evaluating the formation mechanism of the Tibetan Plateau. Various models have been proposed to reveal the structural relationship, although controversies remain. To address these issues, we analysed the seismic and lithologic data of the Kunbei fault system (i.e. the Kunbei, Arlar and Hongliuquan faults), which lies to the north of the Qimen Tagh-Eastern Kunlun Range within the SW Qaidam Basin. Based on the regional geological framework and our kinematic analyses, we propose that the Cenozoic tectonic evolution of the Kunbei fault system can be divided into two stages. From the Early Eocene to the Middle Miocene, the system was characterized by left-lateral strike-slip faults and weak south-dipping thrust faults based on the flower structure in the seismic section, which is an apparent strike-slip deformation that was identified in the −1510-ms time slice and the root-mean-square amplitude attribute slice. This strike-slip motion was generated by the uplift of the Tibetan Plateau caused by the onset of the Indian-Eurasian collision. Since the Middle Miocene, the Kunbei fault system has undergone intense south-dipping thrusting, and a nearly 2.2-km uplift has been observed in the hanging wall in the Arlar fault. The south-dipping thrusting is the far-field effect of the full collision that occurred between the Indian-Eurasian plates. The lake area in the SW Qaidam Basin has been shrinking since the Middle Miocene and presents widespread delta and fluvial deposits, which are consistent with the proposed tectonic evolution.

Keywords Cenozoic · SW Qaidam Basin · Tibetan plateau · Tectonic · Sedimentation

Introduction

The uplift of the Tibetan Plateau is an important geological event that has been the subject of considerable debate for decades (Molnar and Chen 1983; Shackleton et al. 1984; Miller et al. 1987; Kroon et al. 1991; Raymo and Ruddiman 1992; Rea et al. 1998; Yin and Harrison 2000; Soofi and King 2002; Johnson 2002; Wang et al. 2012) and is important for evaluating the Indian-Eurasian collision. Despite its importance in determining the dynamics of deformation, the models that have been proposed to reveal the Cenozoic deformation of the Tibetan Plateau remain controversial (Raymo and Ruddiman 1992; Rea et al. 1998; Yin and Harrison 2000; Soofi and King 2002; Johnson 2002; Wang et al. 2012).

The Qaidam Basin and Qimen Tagh-Eastern Kunlun Range in the northern margin of the Tibetan Plateau hold important implications for the growth mechanism of the Tibetan Plateau. Thus, figuring out their tectonic relationship is important for revealing the Cenozoic deformation of the Tibetan Plateau. Fortunately, the Kunbei fault system, which stands out as a Cenozoic tectonic deformation

✉ Chaodong Wu
cdwu@pku.edu.cn

[1] Key Laboratory of Orogenic Belts and Crustal Evolution, Ministry of Education, School of Earth and Space Sciences, Peking University, Beijing 100871, China

[2] Institute of Oil and Gas, Peking University, Beijing 100871, China

[3] Research Institute of Exploration and Development, Qinghai Oilfield Company, PetroChina, Dunhuang 736202, China

[4] Research Institute of Exploration and Development, Northwest Branch, PetroChina, Lanzhou 730020, China

feature, is greatly influenced by the Qimen Tagh-Eastern Kunlun Range and accepted as a natural laboratory for exploring Cenozoic crustal deformation and structure relationship between the Qaidam Basin and Qimen Tagh-Eastern Kunlun Range.

Over the past three decades, a number of models have been proposed to explain the Cenozoic crustal deformation and structure relationship between the Qaidam Basin and Qimen Tagh-Eastern Kunlun Range (Bally et al. 1986; Burchfiel et al. 1989; Song and Wang 1993; Meyer et al. 1998; Metivier et al. 1998; Chen et al. 1999; Mock et al. 1999; Tapponnier et al. 2001; Lin et al. 2002; Jolivet et al. 2003; Zhou et al. 2006; Fu and Awata 2007; Yin et al. 2007, 2008b; Meng and Fang 2008; Wang et al. 2010, 2011a, b, 2012; Cheng et al. 2014; Wu et al. 2014). Burchfiel et al. (1989) and Chen et al. (1999) proposed that the Eastern Kunlun Range was induced by the motion of a major south-dipping thrust and bounded the southern margin of the Qaidam Basin. Mock et al. (1999) expanded the concept of the Eastern Kunlun Range and speculated that the northward thrusting across the Eastern Kunlun Range was associated with vertical wedge extrusion starting at ca. 30–20 Ma. As opposed to the south-dipping thrusting point, Yin et al. (2007) and Wang et al. (2011a, b) proposed that a series of Cenozoic north-dipping faults occurred in the Qaidam Basin and the basin thrusted southward over the Qimen Tagh Mountains. Compared with the above models, Cheng et al. (2014) proposed that the Late Neogene northward growth of the convex northward structures in the Qimen Tagh Range and SW Qaidam Basin was driven by a left-lateral strike-slip motion along the Kunlun fault. While migrating northward, the western segment of the Kunlun fault gradually rotated over time. In addition to the hypotheses described above, scholars have suggested that the Eastern Kunlun Range consists of a large transpressional system that includes the left-slip Kunlun fault in the south and a north-directed thrust along the northern flank of the Eastern Kunlun Range (Meyer et al. 1998; Tapponnier et al. 2001; Jolivet et al. 2003).

To date, the growth mechanism of the Tibetan Plateau and the structural relationships between the development of the Qaidam Basin and Qimen Tagh-Eastern Kunlun Range remain controversial. In this work, we have undertaken a detailed petrographical, stratigraphical and seismic sedimentological analysis of the Kunbei fault system (i.e. Kunbei, Arlar and Hongliuquan faults) from the SW Qaidam Basin to constrain the tectonic relationship between the Qaidam Basin and the Qimen Tagh-Eastern Kunlun Range. It is hoped that information from this study may be useful for revealing the relationships between the uplift pattern of the Tibetan Plateau and the geometry and temporal development of the SW Qaidam Basin.

Geological setting

The Kunbei fault system consists of the Hongliuquan, Arlar and Kunbei faults, which represents important features in the tectonic evolution of the SW Qaidam Basin. Fault traces are not visible at the surface because of the occurrence of widespread modern unconsolidated deposits across this region (Cheng et al. 2015c). The Cenozoic evolution of the Kunbei fault system, which is distributed in parallel to the north of the Qimen Tagh-Eastern Kunlun Range within the SW Qaidam Basin, was greatly influenced by the Altyn Tagh Range to the west and Qimen Tagh-Eastern Kunlun Range to the south (Fig. 1). This system represents a valuable testing ground for unravelling the structural relationships between the SW Qaidam Basin and Qimen Tagh-Eastern Kunlun Range and revealing the growth mechanism of the Tibetan Plateau in the Cenozoic.

Altyn Tagh range and Qimen Tagh-Eastern Kunlun range

The Cenozoic Altyn Tagh Fault system lies along the northwestern edge of the SW Qaidam and has an along-strike length of >1500 km (Fig. 1a; Yin and Harrison 2000; Yin et al. 2002; Wang et al. 2014; Cheng et al. 2015b). The ENE-trending fault links the western Kunlun Range in the south-west and the Qilian Shan Range in the north-east (Burchfiel et al. 1989; Wang 1997; Yue and Liou 1999; Yin and Harrison 2000; Yin et al. 2002; Cheng et al. 2015b). The left-lateral structure of the Altyn Tagh Fault is generally believed to be a reflection of the far-field effect of the initial stage of the India-Asia collision, and it was initiated in the Palaeocene to Middle Eocene (60–45 Ma) (Bally et al. 1986; Yin et al. 2002, 2008a, 2010). All of the viable pre-slip piercing points on the eastern-central Altyn Tagh Fault have a range of common offsets between 350 and 400 km (Wang et al. 2014), indicating a total left-lateral displacement of 375 ± 25 km (Yue et al. 2001; Wang et al. 2014). Although the Quaternary slip rate in the eastern-central part of the Altyn Tagh Fault, which was measured using GPS by Zhang et al. (2004), was 5.6 ± 1.6 mm/yr, additional dating and reinterpretations have led to a revision of the fault slip rate to approximately 10 mm/yr (Cowgill 2007; Zhang 2007), which is consistent with the long-term geologic rate of the fault over tens of millions of years (Shen et al. 2001; Yin et al. 2002, 2010).

The Eastern Kunlun Range is located in the north-eastern Tibetan Plateau at an average elevation of approximately 5000 m. Both morphologically and tectonically, this range separates the Hoh Xil Basin to the south from the Qaidam Basin to the north (Cheng et al. 2015a). The Eastern Kunlun Range consists of a series of valleys and ranges, such as

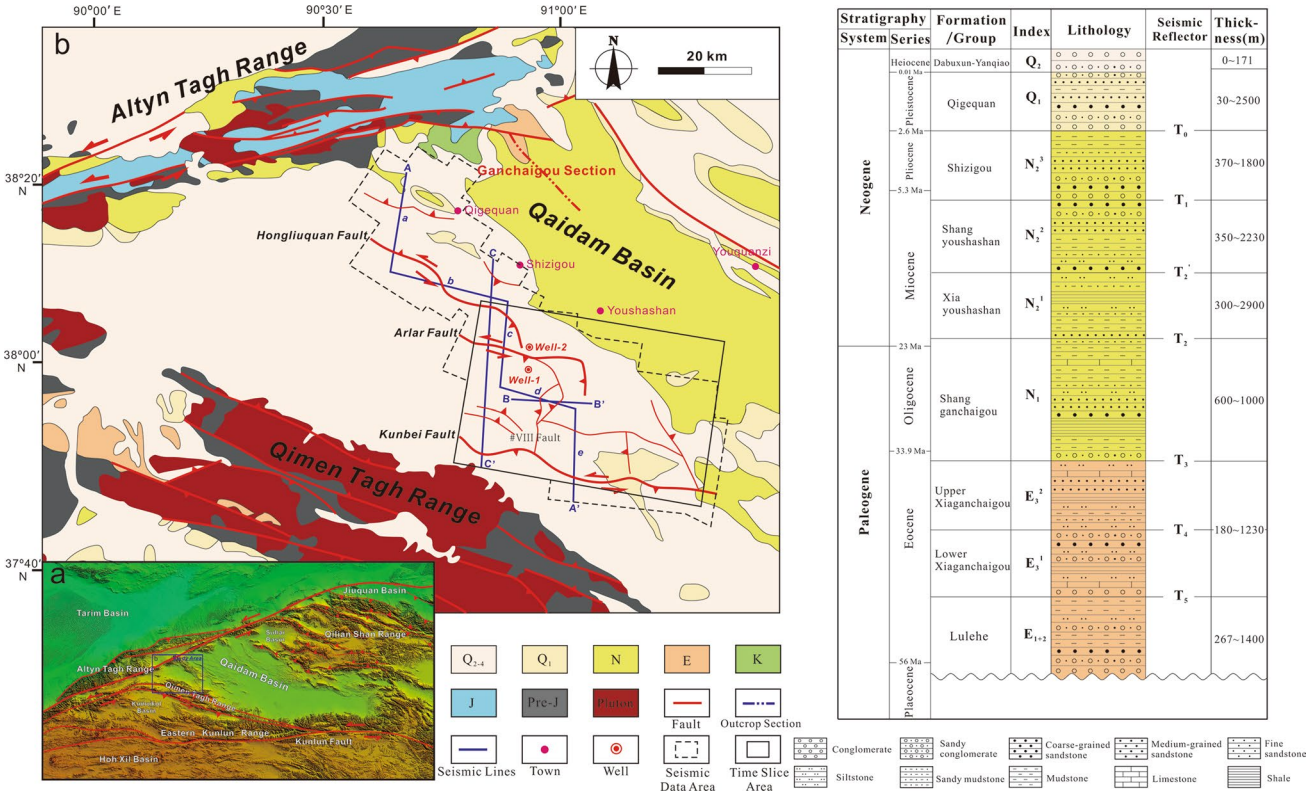

Fig. 1 Geological map and Cenozoic stratigraphic column of the SW Qaidam Basin. The three major faults (Kunbei fault, Arlar fault and Hongliuquan fault) and seismic section locations are indicated on the map. Modified from the Qaidam Basin 1:1,000,000 geological map

the Qimen Tagh Range, Adatan Valley and Kumukol Basin. The onset time of uplift of the Eastern Kunlun Range varies from the Eocene to Miocene (Mock et al. 1999; Jolivet et al. 2001; Yin et al. 2007, 2008b; Wang et al. 2008; Clark et al. 2010; Duvall et al. 2013), and the range reached high altitudes during the Oligocene and early Miocene (Dai et al. 2013; Wang et al. 2014). The Qimen Tagh range has a general WNW–ESE elongated shape (Fig. 1). To the NW, it bends sharply with a south-westward trend subparallel to the Altyn Tagh Range, which lies directly to the north. To the SE, the Qimen Tagh Range converges with the Eastern Kunlun Mountains (Cheng et al. 2014). The sharp contact between the Qaidam Basin and the Qimen Tagh Range has been interpreted as evidence of active north-directed thrusting (Meyer et al. 1998; Jolivet et al. 2003).

SW Qaidam Basin

The Altyn Tagh Range to the north-west and the Qimen Tagh-Eastern Kunlun Range to the south bound the SW Qaidam Basin. The Cenozoic sedimentary filling characteristics and evolutionary processes of the SW Qaidam Basin were influenced by the Altyn Tagh and Kunlun boundary faults along the margins and the Hongliuquan, Arlar and Kunbei faults within the basin. The SW Qaidam Basin experienced multi-stage tectonic activities in the Cenozoic (Fu and Awata 2007; Wang et al. 2010; Cheng et al. 2014, 2015c; Wu et al. 2014). Among the tectonic units, the NW-trending and NE-trending faults dominate the SW Qaidam Basin. The Kunbei fault system includes the Kunbei, Arlar and Hongliuquan faults, which are the major NW-trending faults in the area, and they played key roles in the tectonic evolution and sedimentary filling of the basin. In addition, several NE-trending faults, including the #III, #VIII and other faults, are adjusting faults that influenced the development of the regional strata and faulted blocks.

During the Cenozoic, the basin underwent formation, development and shrinkage stages. Based on magnetostratigraphic evidence, the lithostratigraphic formations from the oldest to the youngest in the Qaidam Basin are divided into the Lulehe Formation (Early–Middle Eocene; Rieser et al. 2006), Lower Xiaganchaigou Formation (43–37.8 Ma; Zheng et al. 2006; Sun et al. 2007; Pei et al. 2009), Upper Xiaganchaigou Formation (37.8–35.5 Ma; Sun et al. 2005b, 2007; Pei et al. 2009), Shangganchaigou Formation (35.5–22 Ma; Sun et al. 2005b; Lu and Xiong 2009), Xiayoushashan Formation (22–15 Ma; Fang et al. 2007; Lu and Xiong 2009), Shangyoushashan Formation (15–8 Ma; Fang et al. 2007), Shizigou Formation (8–2.5 Ma; Fang et al.

Fig. 2 Digital photographs from the SW Qaidam Basin. **a** Picture of the upper XGCG Formation showing widespread lacustrine marl and calcareous mudstones. Ganchaigou field section. See Fig. 1 for the location of Ganchaigou. **b** Picture of the SGCG Formation, which is dominated by lacustrine marl and calcareous silty mudstones. Ganchaigou field section. **c** Picture of the XYSS Formation showing the coarse clastic fan delta deposits. Ganchaigou field section. **d** Picture of the SYSS Formation showing the sedimentary characteristics of the braided rivers. Youshashan. See Fig. 1 for the location of Youshashan

2007) and Qigequan Formation (2.5 Ma–present; Fang et al. 2007).

The Lulehe (LLH) Formation is distributed across most of the SW Qaidam Basin and generally dominated by brownish-red coarse clastic sediments. Borehole data show an upward-fining succession in the LLH Formation, with the lower part containing coarse to pebbly sandstones that gradually grade upward into medium-fine sandstones and mudrocks.

The Xiaganchaigou (XGCG) Formation exhibits a distinct upward-fining succession. Based on the lithological characteristics, the XGCG Formation can be divided into lower and upper members. The thickness of the lower member increases gradually from east to west and from north to south. This member is characterized by brownish-red sandstone–conglomerate assemblages and a basal conglomerate horizon throughout the basin. The upper member is obviously thicker than the lower member and has a maximum thickness of over 1400 m, indicating an apparent increase in the sedimentation rate of the SW Qaidam Basin. The extent of the lake reached its maximum during the deposition of the upper XGCG Formation, during which extensive lacustrine marl and calcareous mudstones were deposited (Fig. 2a). The detrital components of these deposits in the Ganchaigou section are composed of quartz, lithic fragments, feldspar and a small amount of calcite (Fig. 3a). The increased amount of quartz indicates long transportation distances resulting from the transition of the sedimentary environment to a relative stable lacustrine environment.

The Shangganchaigou (SGCG) Formation inherited the sedimentary characteristics of the upper XGCG Formation, including lacustrine marl and calcareous silty mudstones (Fig. 2b), although the lacustrine depositional area has decreased to some extent. The SGCG Formation is generally dominated by sandstones and conglomerates on the margins and transitions rapidly to dark grey mudstones or argillaceous carbonate rocks towards the centre of the basin. The detrital components of the SGCG Formation show slight changes relative to the XGCG Formation and present decreased quartz content and increased feldspar content (Fig. 3b).

The overlying Xiayoushashan (XYSS) Formation is dominated by conglomerates on the margins and sandstones interlayered with variegated mudstones and marlstones in

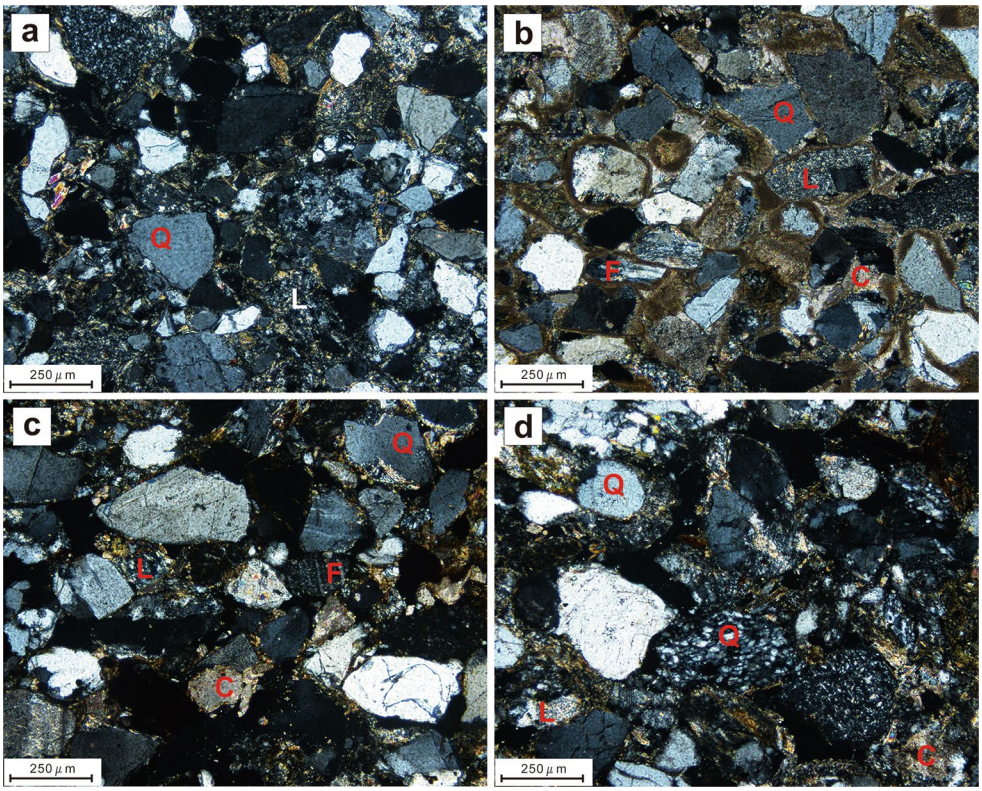

Fig. 3 Photomicrographs of the middle Eocene to Miocene sandstones from the Ganchaigou section in the SW Qaidam Basin. **a** Lithic quartz sandstone from the upper XGCG Formation; **b** Feldspathic quartz sandstone from the SGCG Formation; **c** Feldspathic quartz sandstone from the XYSS Formation; **d** Lithic quartz sandstone from the SYSS Formation. All photographs are shown in orthogonal polarized light. Abbreviation of minerals: *Q* quartz, *F* feldspar, *L* lithic fragment, *C* calcite, *M* matrix

the centre of the basin. Widespread coarse-grained depositions associated with fan delta and fluvial depositions developed (Fig. 2c), indicating a rapid accumulation of sediment. Obvious changes occur among the detrital components of the XYSS Formation (Fig. 3c), with the quartz content remaining high and the feldspar content increasing. Compared with the sediments in the SGCG Formation, the argillaceous matrix is significantly increased. Additionally, the low roundness and sorting of the detrital components may reflect a rapid accumulation of particles.

In comparison, the overlying Shangyoushashan (SYSS) Formation is thinner and contains much coarser deposits. The SW Qaidam Basin is dominated by braided rivers and delta sediments (Fig. 2d), with a massively shrunken basin. The sediments in the Youshashan section exhibit the typical river-binary structure, with a coarse sandy conglomerate deposited at the bottom and a fine-grained deposition above. The detrital components of the SYSS Formation are primarily quartz and lithic fragments (Fig. 3d), with the sorting and roundness of the clastic constituent further decreasing.

The Shizigou (SZG) Formation is composed of grey and yellowish-grey conglomerates along the basin margins. In contrast, a succession of greyish-brown and yellowish-grey mudstones with carbonaceous mudstones is deposited in the centre of the basin. Compared with the underlying XYSS Formation, this formation includes minor carbonate rocks intercalated with white salts and dark grey gypsums.

In conclusion, the Cenozoic deposits in the SW Qaidam Basin are dominated by widespread fine-grained sediments from the LLH to SGCG Formations. The coarse-grained deposition associated with the fan delta and fluvial depositions developed as the basin has shrank since the XYSS Formation.

Data and methods

Three-dimensional seismic data consisting of 13 secondary three-dimensional seismic data covering almost the entire area of the SW Qaidam Basin were applied in our study. The area covered by the three-dimensional seismic data is up to approximately 1955 km^2. The horizontal sampling interval of the three-dimensional seismic data is 15 m × 15 m. To ascertain the actual tectonic pattern and displacement of the fault, we conducted a time–depth

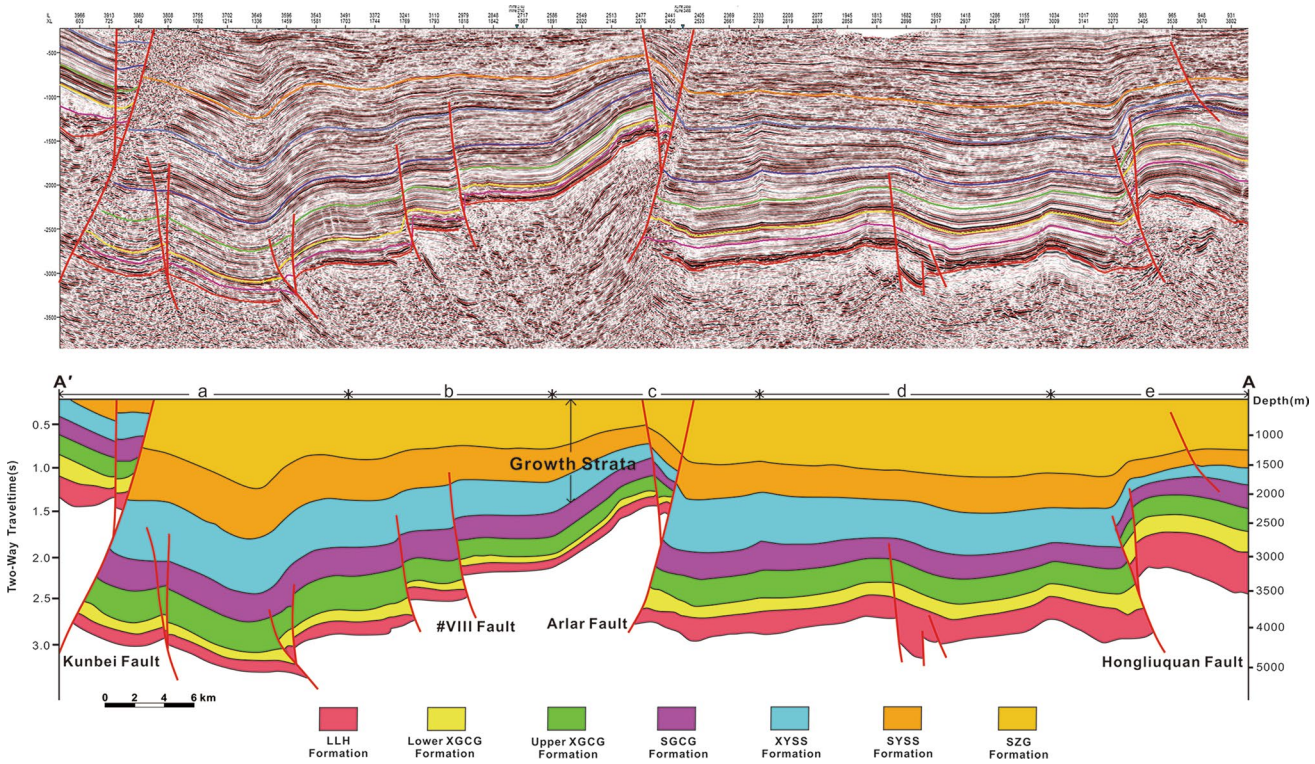

Fig. 4 Seismic section A–A′ intersecting the Kunbei fault system (i.e. the Hongliuquan, Arlar, #VIII and Kunbei faults) in the SW Qaidam Basin. See Fig. 1 for the location. Growth strata and flower structures can be recognized in the Hongliuquan, #VIII, Arlar and Kunbei faults

conversion of the seismic data. First, we produced a synthetic seismogram and established the time–depth relationship between the well logs and seismic data. Depending on the time–depth relationship, we then calculated the average velocity of each key horizon and obtained the velocity model. Finally, we produced the time–depth conversion by taking advantage of the velocity model. To confirm the correctness of these results, we refer to previous works. Our modified results are consistent with the results of Wang et al. (2011a, b), Li (2012) and Cheng et al. (2015c).

The purpose of the seismic exploration is to determine the structure (horizon depth, reservoir thickness, faults, etc.), internal architecture (heterogeneity), petrophysical properties (porosity, permeability, etc.) and hydrocarbon properties (Cosentino and Sabathier 2001). Most seismic interpretations have been performed on vertical and cross lines, and they are then projected onto a time slice (Chopra and Marfurt 2005). A seismic attribute is a quantitative measure of the 3D seismic interpretation. Currently, more than 50 distinct seismic attributes have been calculated from seismic data and applied to the interpretation of geologic structures, stratigraphies and rock/pore fluid properties (Chopra and Marfurt 2005). Horizon amplitude attributes have been introduced (Dalley et al. 2007) to interpret characteristics that are not easily observed in the vertical seismic sections. These amplitude maps are directly related to stratigraphic events and have been used to extrapolate reservoir properties from well controls (Thadani et al. 1987) and sedimentary facies distributions. In this study, we adopt the time slice and horizon root-mean-square (RMS) amplitude attributes to identify changes in the sedimentary facies on both sides of the fault.

Geometry and kinematic features of the Kunbei fault system

The Kunbei fault system consists of three major WNW-trending faults, including the Kunbei fault, the Arlar fault and the Hongliuquan fault (Cheng et al. 2014), and is located at the front of the Qimen Tagh-Eastern Kunlun Range (Fig. 1). The deformation and temporal development of these second-order tectonic units can provide important information regarding the tectonic relationship between the Qaidam Basin and the Qimen Tagh-Eastern Kunlun Range.

Geometric features analysis

The seismic section A–A′ runs from the northern front of the Qimen Tagh Range to the north-western section of the SW Qaidam Basin and intersects the Hongliuquan fault, Arlar fault and Kunbei fault (Fig. 4). The tectonic pattern

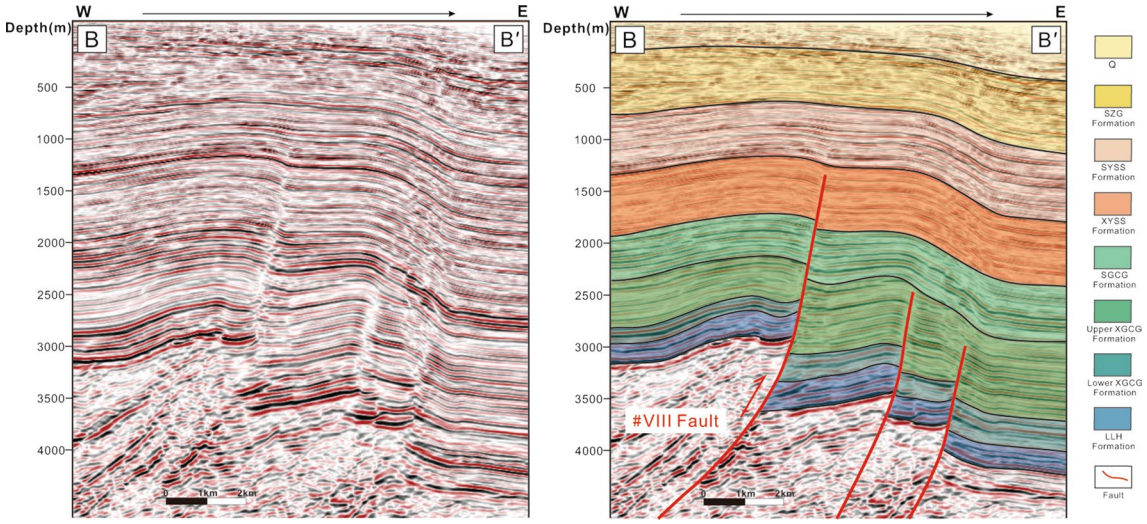

Fig. 5 Seismic section B–B′ intersecting the #VIII fault in the SW Qaidam Basin. See Fig. 1 for the location. The #VIII fault is a high-angle thrust fault, and the fault throw is concentrated below the XYSS Formation, indicating the intense strike-slip motion of the Arlar fault

of section A–A′ is characterized by several high-angle faults with flower structures (Fig. 4). The sediments within the section are Mesozoic to Cenozoic in age.

The Hongliuquan fault is situated in the north-western part of the SW Qaidam Basin and consists of a north-dipping high-angle fault cutting strata from the late Mesozoic to late Cenozoic. The Hongliuquan fault is a reverse fault presenting pre-Middle Miocene strata in the hanging wall that thrust over the strata in the footwall. The apparent vertical fault throw is primarily concentrated between the LLH Formation and the SYSS Formation and clearly indicates the Middle Miocene motion of this fault. The thickness of the Cenozoic strata is constant within each tectonic compartment but varies sharply between the hanging wall and footwall. Combined with the typical flower structure in the pre-Middle Miocene strata, the Hongliuquan fault can be explained by pre-Middle Miocene strike-slip movements and southward thrusting since the Middle Miocene.

The Arlar fault strikes nearly E–W and extends for 84 km. Based on the A–A′ section (Fig. 4), the Arlar fault is a south-dipping high-angle fault (Fig. 4) with an obvious stratigraphic throw of the thickness in each formation on either side of the fault. The fault throw decreases from the bottom to the top of the Cenozoic strata. The stratigraphic thicknesses in the footwall are relatively uniform, whereas the thicknesses in the hanging wall above the XYSS Formation apparently decrease towards the Arlar fault and show typical wedge-shaped growth strata, which demonstrates the northward thrusting motion along the Arlar fault since the Middle Miocene. Similar to the Hongliuquan fault, a positive flower structure is also observed in the Arlar fault, which implies a strike-slip motion. The positive flower structure was generated in the Late Mesozoic strata and occurs in the strata from the Late Mesozoic to the Late Cenozoic, indicating the long-term motion of the strike slip. The strike-slip motion induced a vertical offset of the strata in addition to a thrusting motion.

The #VIII fault is an N–S-trending adjusting fault that developed in the north of the Arlar fault. The B–B′ section (Fig. 5) of the fault indicates that it is a north-west-dipping thrusting fault. The apparent fault throw may have been influenced by the strike-slip movement of the Arlar fault. The strike-slip movement pushed the hanging wall to thrust over the footwall of the pre-Middle Miocene strata.

The Kunbei fault is located to the north of the Qimen Tagh-Eastern Kunlun Range. This fault strikes NW–SE and dips SW over a total length of approximately 134 km. Section A–A′ (Fig. 4) intersects the high-angle Kunbei fault. The apparent fault throw between the two sides of the fault demonstrates that thrusting was dominant. The activity along the Kunbei fault is characterized in the hanging wall by the erosion of the Late Eocene and younger strata and the non-deposition of certain upper Tertiary and Quaternary series (Cheng et al. 2014). Combined with the northward thrusting recognized in the Arlar fault, this erosion may have been caused by the intense northward thrusting in the Middle Miocene. In addition, the steep fault pattern and flower structure demonstrate that the Kunbei fault also experienced strike-slip movement in the Cenozoic.

To summarize, the Hongliuquan, Arlar and Kunbei faults are characterized by high-angle faults, typical flower structures and apparent vertical fault throw. The high-angle fault and typical flower structure may imply strike-slip motion from the Late Mesozoic to Late Cenozoic. The apparent vertical fault throws concentrated between the LLH Formation and SYSS Formation clearly indicate a thrusting

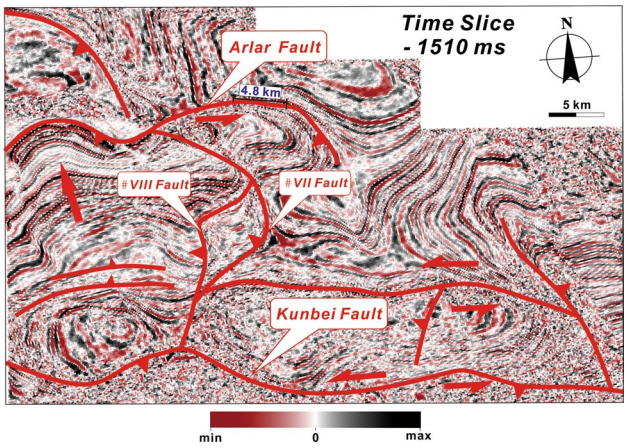

Fig. 6 Time slice (−1510 ms) of the SW Qaidam Basin in the XYSS Formation. The drag structures indicate the strike-slip motion and northward thrusting

motion since the Middle Miocene. Compared with the Arlar and Kunbei faults, the Hongliuquan fault, which presents a north-dipping high-angle fault, is the result of back-thrust facilitated by asymmetric compression. The #VIII fault is a secondary fault that developed to the north of the Arlar fault, and the north-west-dipping thrusting and apparent fault throw may have been influenced by the strike-slip movement of the Arlar fault.

Time slice interpretation

Three-dimensional seismic data provide the opportunity to image stratigraphic records at selected time slices or along interpreted stratigraphic markers (Miall 2002). Such imaging has been used to interpret depositional architecture for a number of years (Miall 2002; Brown 2004). Relatively time-equivalent seismic events are used as a geologic time or chronostratigraphic framework, and phantom slices are created between these framework events using a simplified mathematical model (Zeng 2013).

To further determine the lateral placement of faults, we produced a time slice of −1510 ms. Obvious drag structures associated with the Arlar and Kunbei faults are observed in the time slice (Fig. 6). The strata near the faults were deformed by the strike of the Arlar and Kunbei faults, which may have been induced by the left-lateral strike-slip faulting. A nearly 5-km offset occurs at the end of the Arlar fault because of the sudden deformation along the fault. The strata to the south of the Arlar fault also exhibit obvious deformation that pushed ahead towards the fault, indicating significant northward thrusting. Based on the strata deformation features north-west of the junction between the #VIII fault and the #VII fault, the northward thrusting was posterior to the left-lateral strike-slip faulting. Thus, this area experienced northward thrusting superimposed on the strata that present strike-slip movement.

Amplitude attribute interpretation

Of all the amplitude attributes, the root-mean-square (RMS) amplitude can indicate isolated or extreme amplitude anomalies, and it has been used to track lithologic changes, such as deltaic channels and gas sand (Chen and Sidney 1997; Chopra and Marfurt 2005, 2007). Thus, the different amplitude characteristics of the delta, river channel, submarine fan and other sedimentary facies can be identified from the RMS amplitude slice, which reflects the average amplitude changes in waves within a specific window. To detect the strike-slip behaviour, which was observed in the seismic section, and determine the offset of the Kunbei, Arlar and Hongliuquan faults, we created RMS amplitude slices from the lower XGCG to XYSS Formations.

Various characteristics of the RMS amplitude attribute along the Kunbei, Arlar and Hongliuquan faults are observed in the RMS amplitude attribute slices in the Cenozoic strata (Fig. 7). Although the changes are not clear along every fault in the different formations because of the relatively uniform lithologic characteristics along these faults, the Kunbei, Arlar and Hongliuquan faults are considered to be left-lateral strike-slip faults that occurred in the Cenozoic. Of all of the attribute slices, the slice in the lower XGCG Formation best demonstrates the strike-slip behaviour of the Kunbei strike-slip fault system (Fig. 7a). Along the Hongliuquan fault, the RMS amplitude pattern can be divided into two zones: one for large amplitudes (yellow or green zone) and one for low amplitudes (purple or blue zone). The large amplitude zone is sharply truncated by the fault resulting from the strike-slip movement, and the offset is 6.0–6.2 km (Fig. 7a). Similarly, the offset of the Arlar is approximately 8.8 km (Fig. 7a). The offset of the Kunbei fault cannot be clearly recognized in the lower XGCG Formation because of the poor quality of the seismic data from the front of the Qimen Tagh Range. Fortunately, clear strike-slip behaviour of the Kunbei fault is observed in the XYSS Formation attribute slice, which presents an offset of approximately 9.2 km (Fig. 7c). Figure 7b and d shows the RMS amplitude attribute slices belonging to the upper XGCG Formation and SYSS Formation. The sinistral offset from the lower XGCG Formation to the SYSS Formation decreased successively, implying the long-term movement of the strike slip, and the largest offset cumulated in the lower XGCG Formation. The inconspicuous offset along the Hongliuquan fault in the SYSS Formation was generated by thrusting rather than by the strike-slip movement, implying that the strike-slip movement decreased in the XYSS Formation (Fig. 7d).

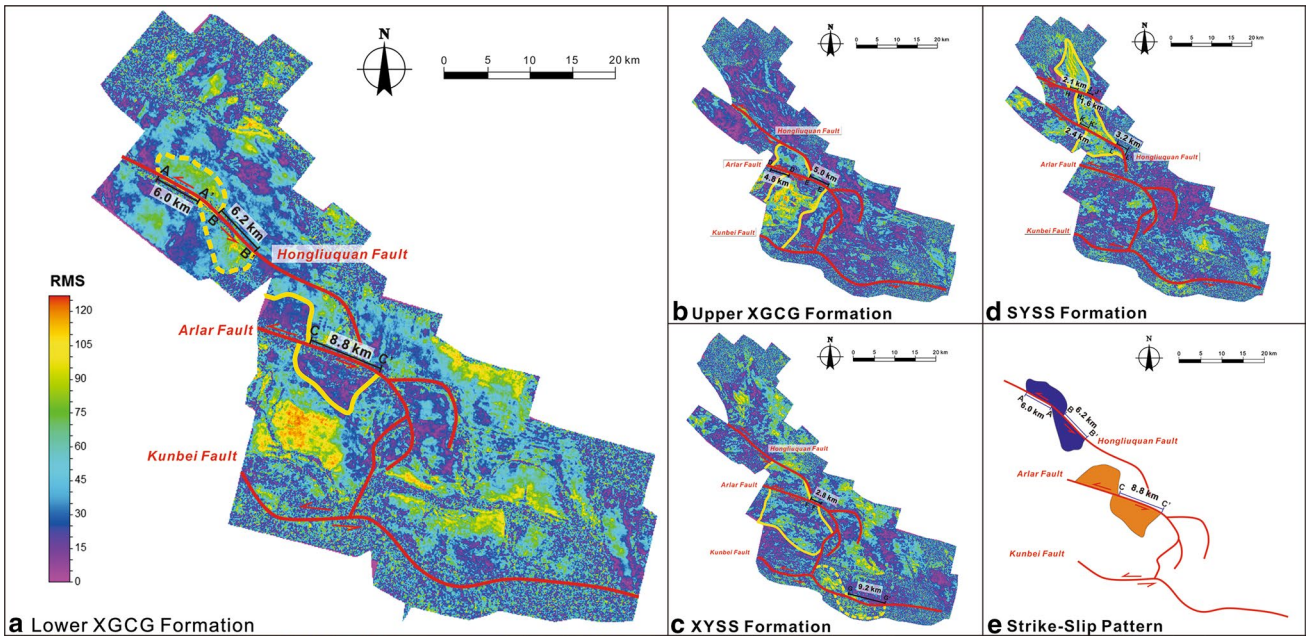

Fig. 7 RMS amplitude attribute slices in the SW Qaidam Basin. **a** Slice of the lower XGCG Formation. **b** Slice of the upper XGCG Formation. **c** Slice of the XYSS Formation. **d** Slice of the SYSS Formation. **e** Strike-slip pattern of the lower XGCG Formation

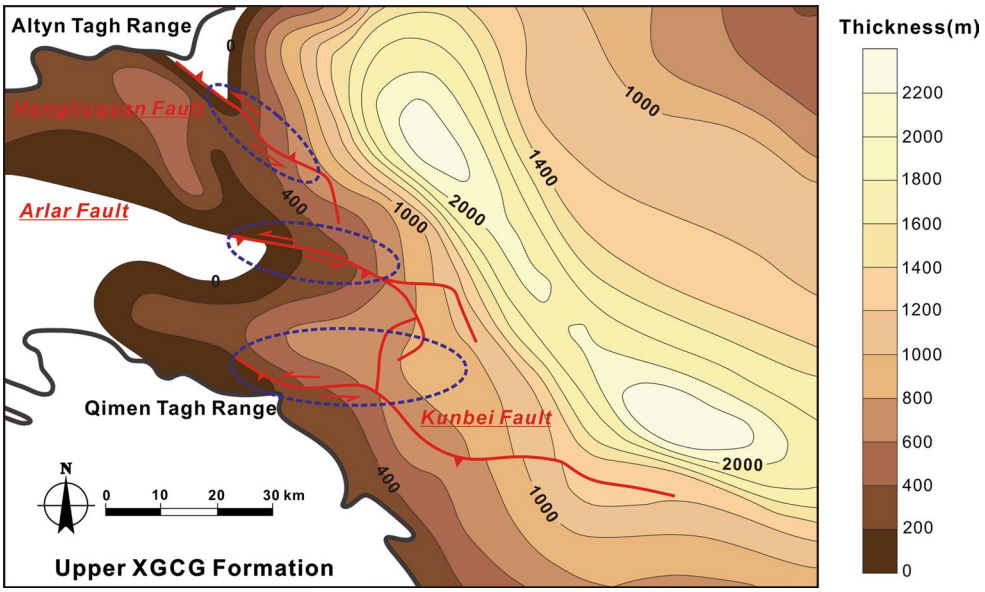

Fig. 8 Isopach map of the upper XGCG Formation. The Kunbei, Arlar, Hongliuquan and #VIII faults are indicated on the isopach map. An apparent offset with a maximum change of approximately 200 m can be observed along these faults

Stratigraphic thickness analysis

Strike-slip movements are known to result in strata thickness variations between the two sides of a fault. To decipher the strike-slip faulting behaviour of the Kunbei fault system, we analysed the isopach map of the upper XGCG Formation to detect the impact of fault motion on the sediment distribution (Fig. 8). The three major faults Kunbei, Arlar and Hongliuquan were marked on the isopach maps produced based on the seismic and drill-hole data. The Kunbei fault system was arranged into a left-lateral right-step en-échelon pattern instead of the usual imbricated pattern of a purely compressive thrust system (Macedo and Marshak 1999; Thomas 2001; McQuarrie 2004; Sepehr and Cosgrove 2004; Cheng et al. 2014). Sharply truncated variations in sediment thickness denoted the offset on either side of the faults. Based on the truncated isopach line, such as the 200- and 400-m isopach lines, the offset of the

three major strike-slip faults can reach tens of kilometres (Fig. 8). Therefore, we infer that the left-lateral strike-slip faulting dominated the Kunbei fault system in or after the Late Eocene.

Discussion

Interpretation of the Kunbei fault system

The Kunbei fault system, located at the front of the Qimen Tagh-Eastern Kunlun Range, holds important implications for the tectonic evolution between the SW Qaidam Basin and the Qimen Tagh-Eastern Kunlun Range. However, there is a lack of consensus on the faults' general properties and evolution, and a convincing explanation is not available (Song and Wang 1993; Yin et al. 2007; Zhou et al. 2006; Wu et al. 2014; Cheng et al. 2014, 2015c). Therefore, studying the Kunbei fault system is of great significance.

Several models have been proposed to explain the tectonic and sedimentary evolution of the Qimen Tagh-Eastern Kunlun Range and Qaidam Basin in recent decades. The northward thrusting model was first proposed by Burchfiel et al. (1989) and then revised by Chen et al. (1999) based on a synthesis of the focal mechanisms and focal depth distributions combined with geological features, which indicate that the Qaidam Basin is limited by a series of south-dipping thrust faults. Therefore, many scholars have suggested that the Qimen Tagh-Eastern Kunlun Range is a transpressional system limited by the Kunlun strike-slip Kunlun fault to the south and a series of south-verging basement thrusts to the north (Jolivet et al. 2001, 2003; Tapponnier et al. 2001; Wang et al. 2006).

However, based on field observations, seismic interpretations and a high-precision deep reflection survey, Yin et al. (2007) proposed the southward thrusting model, which states that a series of Cenozoic north-dipping faults occurred in the Qaidam Basin and the basin thrusted southward over the Qimen Tagh Mountains. Wang et al. (2011a, b) expanded this model and indicated that the initiation of the compressive deformation along the southern margin of the Qaidam Basin is much younger than that along the northern margin of the basin. Compared with the above two models, Cheng et al. (2014) argued that the faults in the northern Kunlun area exhibit regional strike-slip features. The left-lateral movement of the Kunlun fault was initiated in the early Miocene and migrated northward, where it formed a series of left-lateral strike-slip faults (i.e. the Kunbei, Arlar and Hongliuquan faults).

To summarize, despite the large number of models that have been proposed, few studies can yield a convincing hypothesis regarding the relationship between the Qaidam Basin and the Qimen Tagh-Eastern Kunlun Range. Neither the south-dipping thrusting point (Burchfiel et al. 1989; Chen et al. 1999) nor the north-dipping thrusting point (Yin et al. 2007; Wang et al. 2011a, b) can explain the high-angle reverse faults observed in the seismic data (Fig. 4) and the strike-slip behaviour observed in the −1510-ms time slice (Fig. 6), the RMS amplitude slices (Fig. 7) and the isopach map of the upper XGCG Formation (Fig. 8). Wu et al. (2014) indicated that the high-angle reverse faults may have originated from the inversion of pre-existing extensional faults in response to the far-field effect of the Cenozoic India–Eurasia collision, although there is no direct evidence. The strike-slip model proposed by Cheng et al. (2014) considers the left-lateral strike-slip factor; however, it cannot explain the nearly 2.2-km uplift of the Cenozoic strata.

Based on the geometry and kinematic analysis of the Kunbei fault system, we attempt to develop a new convincing explanation. The apparent positive flower structure (Fig. 4), strata deformation along the faults in the time slice (Fig. 6), sharply truncated sediments observed in the RMS amplitude attribute slices (Fig. 7) and sudden variation in sediment thickness indicated by the offset of the isopachs on both sides of the Arlar and Kunbei faults (Fig. 8) reveal that long-term strike-slip motion occurred throughout the Cenozoic. However, the positive flower structure of the Hongliuquan fault is in the pre-Middle Miocene strata, implying the decrease in strike-slip faulting in the Middle Miocene.

The above analysis indicates that the Kunbei fault system is a series of strike-slip faults that occurred during the Cenozoic. However, growth strata, which are closely related to thrusting, can be observed in the A–A′ section. Previous studies have suggested that the growth strata were caused by the northward thrusting, which has been active since the early Cenozoic (Song and Wang 1993; Zhou et al. 2006; Wang et al. 2012; Wu et al. 2014). However, growth strata occur in the post-XYSS Formation, which is inconsistent with previous studies. To determine the time period when rapid thrusting occurred and its duration in the Cenozoic, balanced sections based on the seismic reflection profile data are produced. We re-emerge the evolution of sections C–C′ by each formation in the basin (Fig. 9). The balanced sections of the Cenozoic show that the flower structure occurs in all of the formations, which implies the occurrence of strike-slip activities throughout the Cenozoic. The strata on either side of a fault should have a relatively uniform thickness. Emerging from the balanced section, the strata thickness before the XYSS Formation decreased from north to south across the Hongliuquan fault and had an apparent vertical fault throw between the hanging wall and footwall, and these properties are also observed in the Arlar and Kunbei faults. The different rates of deposition may have caused the thickness

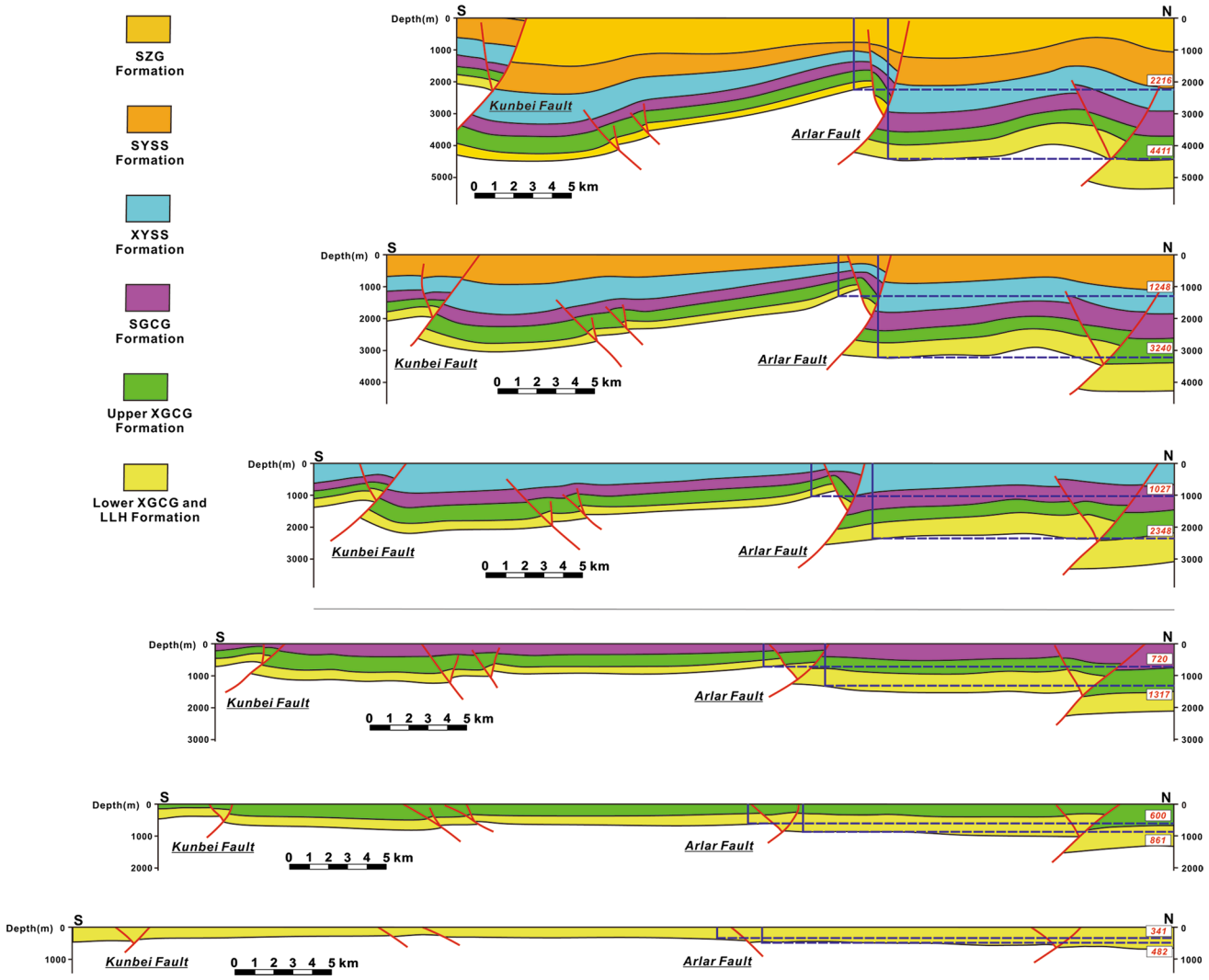

Fig. 9 Evolution of sections C–C′ by each formation in the basin. Apparent growth strata and thrusting can be observed in the XYSS Formation

variations across faults to some extent. However, this difference could not have caused the stepwise changes in the strata thickness. The formations before the XYSS Formation are flat and do not indicate south-dipping thrust fault activities. Combined with the typical flower structures, we determined that the apparent thickness variations across the fault were mainly caused by left-lateral strike-slip movement. Generally, the sedimentary strata in the centre of the basin are thicker than those in the margin of the basin. The thicker sedimentary strata closer to the centre of the basin are transferred from the east, which can explain the stepwise changes in strata thickness. The sedimentary strata of the XYSS Formation show typical wedge-shaped growth strata that present apparently decreasing thicknesses in the hanging wall towards the Arlar fault, which is closely associated with the south-dipping thrusting. To illustrate this change objectively, we measured the thickness across the Arlar Fault in every formation and calculated the thickness differences. The Cenozoic stratigraphic thickness difference between the hanging wall and footwall was up to approximately 2.2 km according to the corresponding measured thicknesses (Fig. 9). Before the XYSS Formation, the apparent thickness variations across the Arlar fault were mainly caused by the strike-slip movement, which resulted in a vertical elevation of approximately 0.6 km (Fig. 10). Massive strata uplift mainly occurred above the SGCG Formation, which presented a nearly 1.6-km vertical elevation (Fig. 10). However, certain vertically elevated strata may also have resulted from the accompanying strike-slip movement.

Synthesizing the above analysis, we propose that the Kunbei fault system (i.e. the Kunbei, Arlar and Hongliuquan faults) is characterized by strike-slip movement throughout the Cenozoic. Intense northward thrusting has

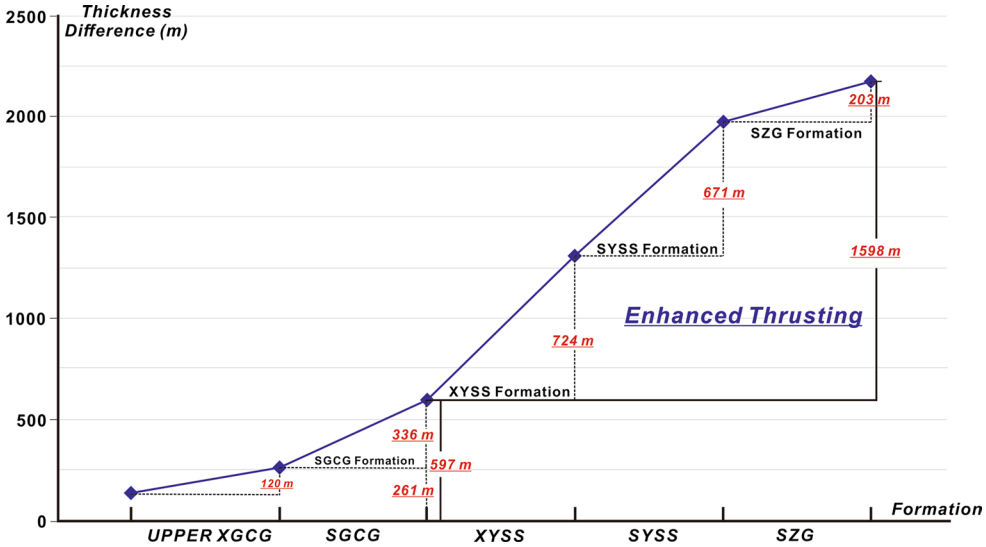

Fig. 10 Stratigraphic thickness difference between the hanging wall and the footwall in the Cenozoic. The apparent thickness variations occurred in the Miocene, implying the enhanced south-dipping thrusting

occurred since the Middle Miocene and caused the huge strata uplift.

Tectonics control on deposition in the SW Qaidam Basin

The Cenozoic Qaidam Basin experienced multi-stage tectonic activities in the Cenozoic (Fu and Awata 2007; Wang et al. 2010; Cheng et al. 2014, 2015c; Wu et al. 2014), and the sedimentary characteristics are consistent with the evolution of the tectonic mechanism. The tectonic activity in the pre-Middle Miocene was not intense, and strike-slip faulting dominated, which is consistent with the expansion of the lacustrine basin and the widespread fine-grained deposits. In the Middle Miocene, the Tibetan Plateau experienced rapid uplift and the Qimen Tagh-Eastern Kunlun Range (Dai et al. 2013; Wang et al. 2014) experienced a complete uplift. In addition, rapid northward thrusting dominated the Kunbei fault system. Under this condition, the lacustrine area narrowed significantly and led to the establishment of widespread delta and fluvial systems in the SW Qaidam Basin.

The strike-slip behaviour of the Kunbei fault system lasted throughout the Cenozoic. Allen and Allen (2013) noted that some of the world's best known strike-slip faults, such as the San Andreas and North Anatolian faults, commonly have startling geomorphic expressions. Alluvial fans accumulate downstream of the range front and may present laterally displaced apices, and stream channels on the fan surface may become beheaded. Geomorphic evidence for strike-slip tectonics is classically displayed along the San Andreas system of California (Wesson et al. 1975; Keller et al. 1982) and along the Hexi Corridor of north-central China (Li and Yang 1998). In the Cenozoic, especially from the Early Eocene to the Middle Miocene, the Kunbei fault system was dominated by a left-lateral strike slip. The left-lateral strike-slip movement also caused asymmetry in the facies patterns across the strike-slip fault.

Sedimentary facies can be identified from the lithological facies. Well-l and Well-2 are located on either side of the Arlar fault, and the sedimentary facies in the SGCG Formation and the XYSS Formation show different characteristics (Fig. 11). The apparent changes in the sedimentary facies of the SGCG Formation in Well-1 are obvious. The lower SGCG Formation (1370–1481 m) primarily contains lacustrine deposits, such as dark mudstones and fine sandstones, whereas the upper portion (1198–1370 m) contains brownish-red sandstone intercalated with conglomerate, which indicates an alluvial fan sedimentary environment. However, the sedimentary environment of the SGCG Formation (2309–2708 m) in Well-2 is relatively constant and results in lacustrine deposits throughout the formation. The apex of the alluvial fan may be sharply truncated by the strike-slip fault and displaced laterally. This characteristic is a convincing indicator of strike-slip movement. The sedimentary environments of the XYSS Formation in Well-1 and Well-2 are relatively uniform, especially for fluvial deposition sedimentary environments. This relative uniformity implies a decreased strike-slip movement. The high sedimentation rate also restrained the exhibition of strike-slip characteristics, such as the asymmetry of facies patterns and strike-slip displacement, as well as the movement of the strike slip.

The analysis of the tectonic activities and sediment in the SW Qaidam Basin suggests major control of the tectonic processes during basin filling as documented above. In turn, the depositional records provide a useful archive for deciphering the tectonic behaviour and evolution of the SW Qaidam Basin.

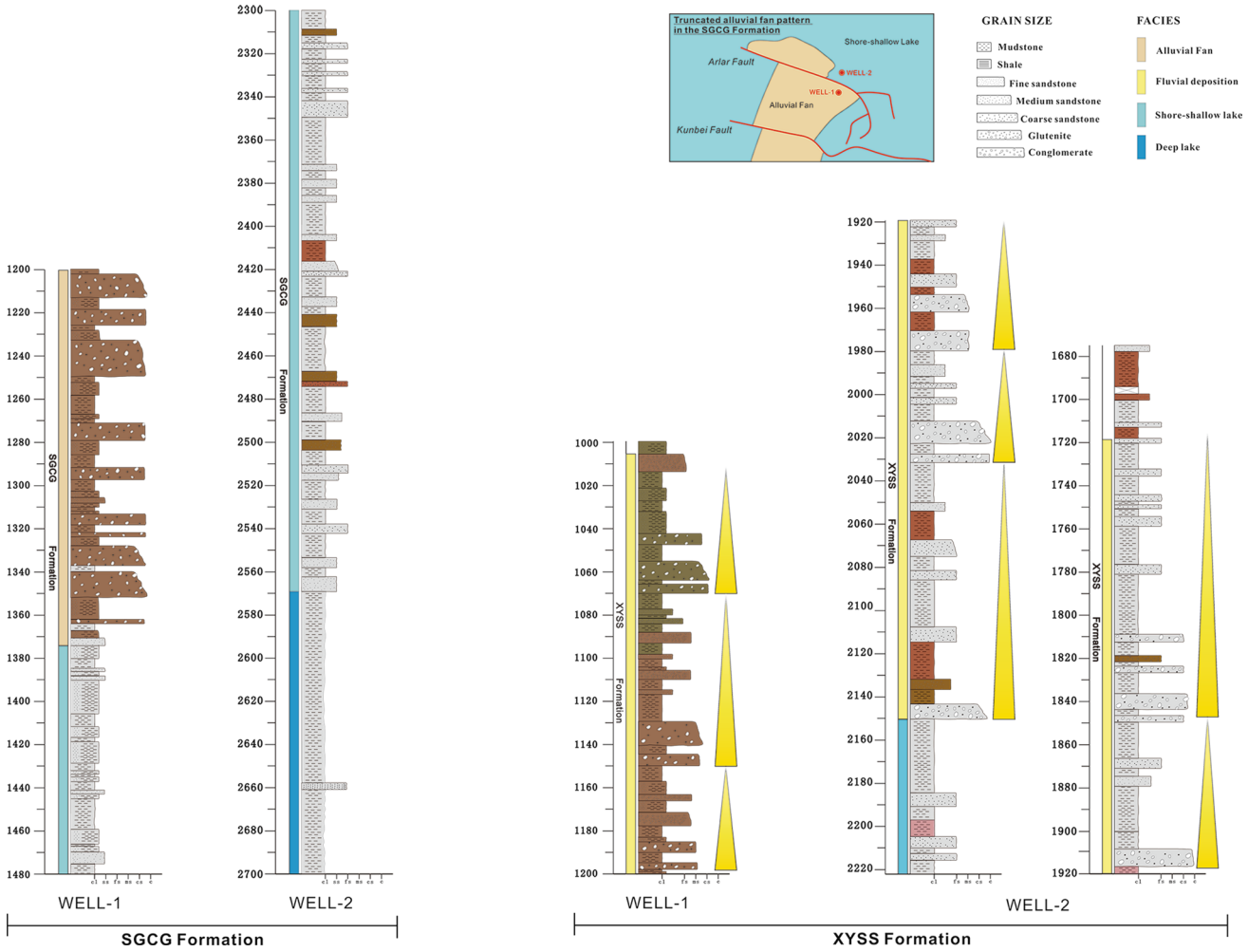

Fig. 11 Cenozoic stratigraphic column of the SGCG and XYSS Formations in Well-1 and Well-2. See Fig. 1 for the well locations. The data were acquired by the Qinghai Oilfield Company (China)

Two-stage evolution of the Kunbei fault system

According to the above analysis, we have determined the Cenozoic geometrical characteristics of the Kunbei fault system. However, the spatial and temporal response of the strike-slip and thrusting behaviour to the uplift of the Tibetan Plateau are still open for discussion.

The Tibetan Plateau is generally regarded as reflecting the Indian-Eurasian collision that started in approximately 55 Ma (Molnar and Chen 1983; Shackleton et al. 1984; Miller et al. 1987; Jijun 1991; Kroon et al. 1991; Raymo and Ruddiman 1992; Rea et al. 1998; Zhisheng et al. 2001; Johnson 2002; Soofi and King 2002; Wang et al. 2014), with the full collision occurring from the Eocene to the Miocene (Molnar and Tapponnier 1975; Klootwijk and Peirce 1979; Patriat and Achache 1984; Patzelt et al. 1996; Wu et al. 2008). The Indian-Eurasian collision may have resulted in crustal shortening (Patriat and Achache 1984; Ratschbacher et al. 1994; Yin and Harrison 2000; Dupont-Nivet et al. 2004) and strike-slip faulting (Tapponnier et al. 1986, 2001; Yin et al. 1994; Dupont-Nivet et al. 2004).

Surface uplift caused by thrusting is well developed in the basins around the Tibetan Plateau, such as the Hoh Xil Basin, Qaidam Basin and Jiuquan Basin. The Qaidam Basin is separated from the Hoh Xil Basin by the Eastern Kunlun Range and from the Jiuquan Basin by the Qilian Shan Range (Fig. 1a; Yin and Harrison 2000). Based on a balanced section of 5 seismic profiles, Wang et al. (2010) reconstructed the Cenozoic deformation history of the Qaidam Basin and indicated that the Qaidam Basin experienced two intensive tectonic deformations, with the first phase occurring from the Middle Eocene to Early Miocene and the stronger second phase occurring from the Middle Miocene to the present. The two stages are consistent with the initial and full Indian-Eurasian collision. Based on the anisotropy of the magnetic susceptibility, Yu et al. (2014)

showed that the Qaidam Basin has experienced at least two periods of compression during the Cenozoic: an early N–S-trending strain no later than the Oligocene and a late NE–SW-trending strain since the Miocene. Coincidentally, Cheng et al. (2015b) estimated that the initial movement along the Altyn Tagh fault occurred broadly between the Eocene and Miocene Epochs (Chen et al. 2001; Meng et al. 2001; Wan et al. 2001; Yue et al. 2001; Yin et al. 2002; Robinson et al. 2003; Wu et al. 2012a, b) and the left-lateral slip of the Altyn Tagh fault accelerated in the early Miocene.

Similar to the Qaidam Basin, the uplift history of the Tibetan Plateau is recorded in the Jiuquan Basin and Hoh Xil Basin. The Jiuquan Basin is a foreland basin, and the southern boundary is formed by the Qilian Shan fold and thrust belt, which separates the Jiuquan Basin from the Qaidam Basin. The basin's development can be divided into a strike-slip basin stage (37.7–30.3 Ma) and a thrust foreland basin stage (29.5–0 Ma; Wang et al. 2014). During the thrust foreland basin stage, the strata consisted of several coarsening-upward sequences, which indicate that the basin was a foreland basin controlled by faults along the thrust front of the North Qilian Shan. The initiation of the uplift in southern Qilian Shan might have occurred at approximately 30 Ma based on its cooling history (Jolivet et al. 2001; Wang 2004). However, the rapid cooling of northern Qilian Shan began in 8–9.5 Ma (Zheng et al. 2010; Wang et al. 2014). Hoh Xil is also a foreland basin that was uplifted, and it formed the northern part of the Tibetan Plateau in the Eocene and Early Oligocene under the influence of Fenghuo Shan-Nangqian thrusting, which was caused by the onset of the India-Asia collision (Liu and Wang 2001; Horton et al. 2002; Spurlin et al. 2005; Zhu et al. 2006). In summary, the Miocene was a critical period in the tectonic evolution of the Tibetan Plateau and basins around (Yue and Liou 1999; Kirby et al. 2002, 2007; Ding et al. 2004; Sun et al. 2005a; Wang et al. 2010, 2012; Yu et al. 2014; Cheng et al. 2015b).

Combined with the points mentioned above, we propose that the tectonic evolution of the Tibetan Plateau and the surrounding tectonic zones can be divided into two stages that are consistent with the initial and full Indian-Eurasian collision. Yang et al. (2007) indicated that the concomitant uplift with strike-slip faults is a result of the restraining bend during the oblique collision of plates. The oblique collision of the India and Eurasian plates caused the basement-involved structure to express certain features, such as a strike-slip and thrust fault (Xie et al. 1998; Xiao et al. 1998; Yang 1999). The Eocene–Middle Miocene crustal shortening and strike-slip faulting in the north-eastern margin of the Tibetan Plateau are associated with the initial Indian-Eurasian collision. From the Middle Miocene, regional rather than local rapid uplift and fast exhumation

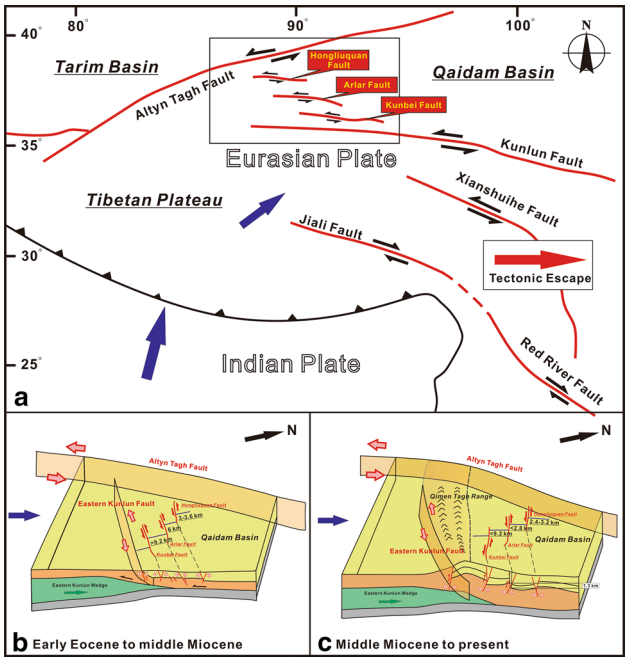

Fig. 12 Genetic model of the Kunbei fault system in the Cenozoic. *a* Sketch map of strike-slip fault in the plane and the escape structures. *b* Genetic model of the Kunbei fault system before the Middle Miocene. The offset before the Middle Miocene are determined based on the offset of the lower XGCG Formation by subtracting the offset in the stratum of the Middle Miocene. The offsets are identified in the RMS amplitude slices. *c* Genetic model of the Kunbei fault system from the Middle Miocene to the present. The stratigraphic thickness difference between the hanging wall and footwall is based on the balanced section

of the north-eastern Tibetan Plateau have occurred under the far-field effect of the full Indian-Eurasian collision.

Early Eocene to Middle Miocene: dominated by strike-slip deformations

The Indian-Eurasian plates began to collide in the Early Eocene and caused plateau building and strike-slip extrusions towards the east and north-east (Tapponnier et al. 2001). The extrusion stress accompanying the initial collision was released by the widespread strike-slip movements. Thus, the margin of the Tibetan Plateau was dominated by strike-slip extrusions, which generated a series of strike-slip faults, such as the Altyn Tagh left-lateral strike-slip fault, Red River right-lateral strike-slip fault and Eastern Kunlun left-lateral strike-slip fault (Fig. 12a). Under this condition, the Kunbei fault system began to form (Fig. 12b). The Kunbei fault system acted as a series of strike-slip faults during the Cenozoic. Based on the RMS amplitude attribute along the faults, the sinistral offset from the lower XGCG Formation to the SYSS Formation decreased successively, which implies the long-term movement of the strike slip, with the

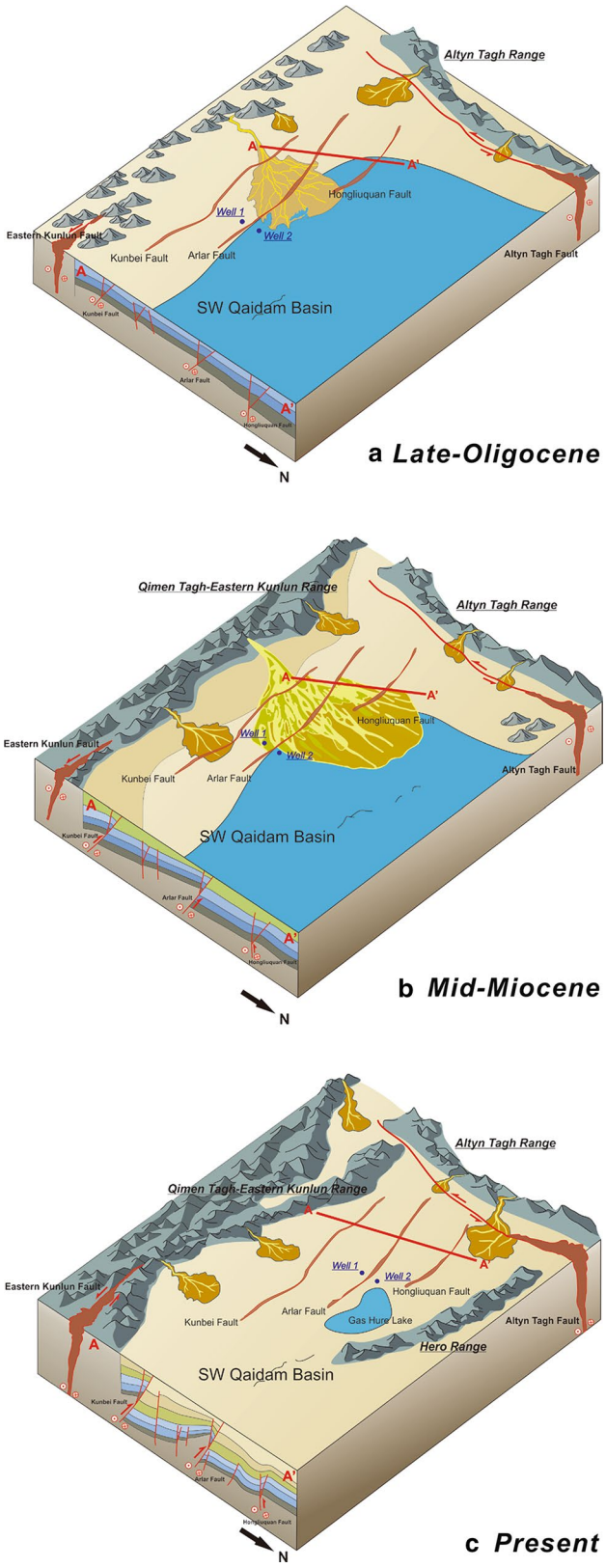

Fig. 13 Schematic drawing showing the tectono-sedimentary framework in the Cenozoic SW Qaidam Basin. **a** Tectono-sedimentary framework in the late Oligocene. The Kunbei fault system was dominated by strike-slip movement and weak south-dipping thrusting. Widespread lacustrine deposits dominated the SW Qaidam Basin. **b** Tectono-sedimentary framework in the Middle Miocene. South-dipping thrusting of the Kunbei fault system was markedly enhanced in the Middle Miocene. The Qimen Tagh-Eastern Kunlun Range experienced rapid uplift and reached high altitude at that time. Corresponding to the tectonic evolution of the Kunbei fault system and Qimen Tagh-Eastern Kunlun Range, delta deposits developed in the SW Qaidam Basin. **c** Tectono-sedimentary framework of the present SW Qaidam Basin

largest offset cumulated in the lower XGCG Formation. Thus, the offset before the Middle Miocene can be determined based on the offset of the lower XGCG Formation by subtracting the offset in the stratum of the Middle Miocene (Fig. 12a). The three faults formed almost simultaneously. Considering that the Kunbei fault is much closer to the Eastern Kunlun left-lateral strike-slip fault, the Kunbei fault may have formed slightly earlier than the Arlar and Hongliuquan faults. Influenced by the ribbon and dolphin effects, certain changes may have occurred in the strike-slip fault dips. Inevitably, north-dipping backthrust occurred with the strike-slip motion. Consistent with the relatively weak tectonic activities, the SW Qaidam Basin is mainly composed of widespread lacustrine deposits of fine-grained sediments (Fig. 13a).

Middle Miocene to present: dominated by south-dipping thrusting

In the Middle Miocene, full collision occurred between the Indian-Eurasian plates. The intense extrusion stress could not be released by the strike-slip fault movements. Thus, the anabatic collision caused the rapid uplift and fast exhumation of the north-eastern Tibetan Plateau, Eastern Kunlun Range (Yin et al. 2008b; Cheng et al. 2015a) and Qilian Shan (Zheng et al. 2006; Fang et al. 2007; Lu and Xiong 2009; Clark et al. 2010; Lin et al. 2010; Zheng et al. 2010) and accelerated the strike slip of the Altyn Tagh fault (Yue and Liou 1999; Kirby et al. 2002, 2007; Ding et al. 2004; Sun et al. 2005a; Wang et al. 2010, 2012; Yu et al. 2014; Cheng et al. 2015b). Blocked by the northern Qilian Shan Range, the Arlar and Kunbei faults began to rapidly thrust northward (Fig. 12c). Based on the balanced sections, the Cenozoic stratigraphic thickness difference between the hanging wall and the footwall can reach nearly 2.2 km. A pre-existing strike-slip structure produces thrusting, and high-angle faults are possible.

The growth style for the three faults can be divided into two stages. In the first stage, the three faults mainly developed strike-slip structures, and little northward thrusting may have occurred in the Kunbei fault. In the second stage, the growth style of the Hongliuquan fault was quite different from that of the Arlar and Kunbei faults. Influenced by the full collision of the Indian-Eurasian plates and the

uplift of the Tibetan Plateau, the Arlar and Kunbei faults began to rapidly thrust northward. However, facilitated by the asymmetric compression, the Hongliuquan fault was a backthrust, and the pre-Middle Miocene strata in the hanging wall thrust over the strata in the footwall. Regarding the northward-decreased sinistral offset from the Kunbei fault to the Hongliuquan fault identified from the RMS amplitude slice (Fig. 7), the Kunbei fault system experienced long-term intense strike-slip faulting, which was influenced by the East Kunlun left-lateral strike-slip fault.

In the second stage, the Qimen Tagh Range experienced fast exhumation and the areal extent of lacustrine facies began to shrink and was replaced by widespread coarse-grained deposits associated with fan delta and fluvial depositions (Fig. 13b). The shrinkage of the lake area continues today, and the current SW Qaidam Basin is dominated by non-lacustrine deposits and only presents a small lake area, i.e. the Gas-Hure Lake (Fig. 13c). The Qimen Tagh-Eastern Kunlun Range has experienced a complete uplift.

Conclusions

Based on the geometry and kinematic analysis of the Kunbei fault system, we have shown that the Kunbei fault system and SW Qaidam Basin experienced a two-stage evolution during the Cenozoic. The initial collision of the Indian-Eurasian plates caused plateau building and strike-slip extrusion towards the east and north-east. The Kunbei fault system was closely related to the strike-slip extrusion and characterized by left-lateral strike-slip faults and weak south-dipping thrust faults from the Early Eocene to the Middle Miocene. From the Middle Miocene, the influence of the full collision between the Indian-Eurasian plates and the accompanying rapid uplift of the Tibetan Plateau caused the Kunbei fault system to experience intense south-dipping thrusting, which continues today.

Controlled by the tectonic evolution of the Kunbei fault system, the SW Qaidam Basin has experienced basin formation, stable sedimentation and shrinkage stages. The areal extent of the lacustrine facies in the SW Qaidam Basin has been shrinking since the Middle Miocene, which is consistent with the rapid uplift of the Qimen Tagh-Eastern Kunlun Range and intense south-dipping thrusting of the Kunbei fault system.

Acknowledgments This study was supported by the National Science and Technology Major Project of the Ministry of Science and Technology of China (2011ZX05009-001). We thank Dr. Linlin Li, Dr. Xutao Li, Dr. Chenchen Zhang, Dr. Tianqi Zhou, Master Mengyi Ren and Master Jieyuan Kang for helpful conversations. We would also like to appreciate the Editor-in-Chief Prof. Wolf-Christian Dullo, associate editor Prof. Wenjiao Xiao and the reviewers for the constructive and thoughtful comments that helped improve the manuscript.

References

Allen PA, Allen JR (2013) Basin analysis: principles and application to petroleum play assessment. Wiley, Chichester

Bally AW, Chou I-M, Clayton R, Eugster HP, Kidwell S, Meckel LD, Ryder RT, Watts AB, Wilson AA (1986) Notes on sedimentary basins in China—report of the American Sedimentary Basins delegation to the People's Republic of China. U.S. Geological Survey Open-File Report 108:86–327

Brown AR (2004) Interpretation of three-dimensional seismic data. The American Association of Petroleum Geologists and the Society of Exploration Geophysicists, Tulsa

Burchfiel BC, Deng QD, Molnar P, Royden L, Wang YP, Zhang PZ, Zhang WQ (1989) Intracrustal detachment within zones of continental deformation. Geology 17:748–752

Chen Q, Sidney S (1997) Seismic attribute technology for reservoir forecasting and monitoring. Lead Edge 16:445–448

Chen WP, Chen CY, Nabelek JL (1999) Present-day deformation of the Qaidam basin with implications for intra-continental tectonics. Tectonophysics 305:165–181

Chen ZL, Zhang YQ, Wang XF, Chen XH, Washburn Z (2001) Fission track dating of apatite constrains on the Cenozoic uplift of the Altyn Tagh Mountain. Acta Geoscientia Sinica 22:413–417

Cheng F, Jolivet M, Fu ST, Zhang QQ, Guan SW, Yu XJ, Guo ZJ (2014) Northward growth of the Qimen Tagh Range: a new model accounting for the Late Neogene strike-slip deformation of the SW Qaidam Basin. Tectonophysics 632:32–47

Cheng F, Fu S, Jolivet M, Zhang C, Guo Z (2015a) Source to sink relation between the Eastern Kunlun Range and the Qaidam Basin, northern Tibetan Plateau, during the Cenozoic. Geol Soc Am Bull 128:258–283

Cheng F, Guo ZJ, Jenkins HS, Fu ST, Cheng X (2015b) Initial rupture and displacement on the Altyn Tagh fault, northern Tibetan Plateau: constraints based on residual Mesozoic to Cenozoic strata in the western Qaidam Basin. Geosphere 11:921–942

Cheng X et al (2015c) Geometry and kinematics of the Arlar strike-slip fault, SW Qaidam basin, China: new insights from 3-D seismic data. J Asian Earth Sci 98:198–208

Chopra S, Marfurt KJ (2005) Seismic attributes - A historical perspective. Geophysics 70:3SO-28SO

Chopra S, Marfurt KJ (2007) Seismic attributes for prospect identification and reservoir characterization. SEG Geophysical Developments Series No. 11

Clark MK, Farley KA, Zheng DW, Wang ZC, Duvall AR (2010) Early Cenozoic faulting of the northern Tibetan Plateau margin from apatite (U-Th)/He ages. Earth Planet Sci Lett 296:78–88

Cosentino L, Sabathier JC (2001) Integrated reservoir studies. Institut Français Du Pétrole Publications, Paris

Cowgill E (2007) Impact of riser reconstructions on estimation of secular variation in rates of strike-slip faulting: revisiting the Cherchen River site along the Altyn Tagh Fault, NW China. Earth Planet Sci Lett 254:239–255

Dai JG, Wang CS, Hourigan J, Santosh M (2013) Multi-stage tectono-magmatic events of the Eastern Kunlun Range, northern Tibet: insights from U-Pb geochronology and (U-Th)/He thermochronology. Tectonophysics 599:97–106

Dalley R, Gevers E, Stampfli G, Davies D, Gastaldi C, Ruijtenberg P, Vermeer G (2007) Dip and azimuth displays for 3D seismic interpretation. First Break 25:101–108

Ding GY, Chen J, Tian QJ, Shen XH, Xing CQ, Wei KB (2004) Active faults and magnitudes of left-lateral displacement along the northern margin of the Tibetan Plateau. Tectonophysics 380:243–260

Dupont-Nivet G, Robinson D, Butler RF, Yin A, Melosh HJ (2004) Concentration of crustal displacement along a weak Altyn Tagh

fault: Evidence from paleomagnetism of the northern Tibetan Plateau. Tectonics 23:TC1020

Duvall AR, Clark MK, Kirby E, Farley KA, Craddock WH, Li CY, Yuan DY (2013) Low-temperature thermochronometry along the Kunlun and Haiyuan Faults, NE Tibetan Plateau: evidence for kinematic change during late-stage orogenesis. Tectonics 32:1190–1211

Fang X et al (2007) High-resolution magnetostratigraphy of the Neogene Huaitoutala section in the eastern Qaidam Basin on the NE Tibetan Plateau, Qinghai Province, China and its implication on tectonic uplift of the NE Tibetan Plateau. Earth Planet Sci Lett 258:293–306

Fu BH, Awata Y (2007) Displacement and timing of left-lateral faulting in the Kunlun Fault Zone, northern Tibet, inferred from geologic and geomorphic features. J Asian Earth Sci 29:253–265

Horton BK, Yin A, Spurlin MS, Zhou JY, Wang JH (2002) Paleocene-Eocene syncontractional sedimentation in narrow, lacustrine-dominated basins of east-central Tibet. Geol Soc Am Bull 114:771–786

Jijun L (1991) The environmental effects of the uplift of the Qinghai-Xizang Plateau. Quatern Sci Rev 10:479–483

Johnson MRW (2002) Shortening budgets and the role of continental subduction during the India-Asia collision. Earth Sci Rev 59:101–123

Jolivet M et al (2001) Mesozoic and Cenozoic tectonics of the northern edge of the Tibetan plateau: fission-track constraints. Tectonophysics 343:111–134

Jolivet M et al (2003) Neogene extension and volcanism in the Kunlun Fault Zone, northern Tibet: new constraints on the age of the Kunlun Fault. Tectonics 22:1052

Keller EA, Bonkowski MS, Korsch RJ, Shlemon RJ (1982) Tectonic Geomorphology of the San-Andreas Fault Zone in the Southern Indio Hills, Coachella Valley, California. Geol Soc Am Bull 93:46–56

Kirby E et al (2002) Late Cenozoic evolution of the eastern margin of the Tibetan Plateau: inferences from 40Ar/39Ar and (U-Th)/He thermochronology. Tectonics 21:1001

Kirby E, Harkins N, Wang EQ, Shi XH, Fan C, Burbank D (2007) Slip rate gradients along the eastern Kunlun fault. Tectonics 26:TC2010

Klootwijk CT, Peirce JW (1979) India's and Australia's pole path since the late Mesozoic and the India-Asia collision. Nature 282:605–607

Kroon D, Steens T, Troelstra SR (1991) Onset of monsoonal related upwelling in the western Arabian Sea as revealed by planktonic foraminifers. In: Prell WL, Niitsuma N et al (eds) Proceedings of the ocean drilling program, scientific results, vol 117. Ocean Drilling Program, College Station, Texas, pp 257–263

Li WL (2012) The study of structural characteristics in western Qaidam Basin. Master's Thesis, Southwest Petroleum University (in Chinese with English abstract)

Li YL, Yang JC (1998) Tectonic geomorphology in the Hexi Corridor, north-west China. Basin Res 10:345–352

Lin A, Fu B, Guo J, Zeng Q, Dang G, He W, Zhao Y (2002) Co-seismic strike-slip and rupture length produced by the 2001 Ms 8.1 Central Kunlun earthquake. Science 296:2015–2017

Lin XB, Chen HL, Wyrwoll KH, Cheng XG (2010) Commencing uplift of the Liupan Shan since 9.5 Ma: evidences from the Sikouzi section at its east side. J Asian Earth Sci 37:350–360

Liu ZF, Wang CS (2001) Facies analysis and depositional systems of Cenozoic sediments in the Hoh Xil basin, northern Tibet. Sed Geol 140:251–270

Lu HJ, Xiong SF (2009) Magnetostratigraphy of the Dahonggou section, northern Qaidam Basin and its bearing on Cenozoic tectonic evolution of the Qilian Shan and Altyn Tagh Fault. Earth Planet Sci Lett 288:539–550

Macedo J, Marshak S (1999) Controls on the geometry of fold-thrust belt salients. Geol Soc Am Bull 111:1808–1822

McQuarrie N (2004) Crustal scale geometry of the Zagros fold-thrust belt. Iran. Journal of Structural Geology 26:519–535

Meng Q-R, Fang X (2008) Cenozoic tectonic development of the Qaidam Basin in the northeastern Tibetan Plateau. Geol Soc Am Spec Pap 444:1–24

Meng QR, Hu JM, Yang FZ (2001) Timing and magnitude of displacement on the Altyn Tagh fault: constraints from stratigraphic correlation of adjoining Tarim and Qaidam basins, NW China. Terra Nova 13:86–91

Metivier F, Gaudemer Y, Tapponnier P, Meyer B (1998) Northeastward growth of the Tibet plateau deduced from balanced reconstruction of two depositional areas: the Qaidam and Hexi Corridor basins, China. Tectonics 17:823–842

Meyer B et al (1998) Crustal thickening in Gansu-Qinghai, lithospheric mantle subduction, and oblique, strike-slip controlled growth of the Tibet plateau. Geophys J Int 135:1–47

Miall AD (2002) Architecture and sequence stratigraphy of Pleistocene fluvial systems in the Malay Basin, based on seismic time-slice analysis. Aapg Bull 86:1201–1216

Miller KG, Fairbanks RG, Mountain GS (1987) Tertiary oxygen isotope synthesis, sea level history, and continental margin Erosion. Paleoceanography 2:1–19

Mock C, Arnaud NO, Cantagrel J-M (1999) An early unroofing in northeastern Tibet? Constraints from 40 Ar/39 Ar thermochronology on granitoids from the eastern Kunlun range (Qianghai, NW China). Earth Planet Sci Lett 171:107–122

Molnar P, Chen WP (1983) Focal depths and fault plane solutions of earthquakes under the tibetan plateau. J Geophys Res 88:1180–1196

Molnar P, Tapponnier P (1975) Cenozoic Tectonics of Asia: effects of a Continental Collision: Features of recent continental tectonics in Asia can be interpreted as results of the India-Eurasia collision. Science 189:419–426

Patriat P, Achache J (1984) India Eurasia Collision chronology has implications for crustal shortening and driving mechanism of plates. Nature 311:615–621

Patzelt A, Li HM, Wang JD, Appel E (1996) Palaeomagnetism of Cretaceous to Tertiary sediments from southern Tibet: evidence for the extent of the northern margin of India prior to the collision with Eurasia. Tectonophysics 259:259–284

Pei JL et al (2009) Evidence for Tibetan plateau uplift in Qaidam basin before Eocene-Oligocene boundary and its climatic implications. J Earth Sci 20:430–437

Ratschbacher L, Frisch W, Liu GH, Chen CS (1994) Distributed deformation in southern and western Tibet during and after the India-Asia collision. J Geophys Res-Sol Ea 99:19917–19945

Raymo ME, Ruddiman WF (1992) Tectonic forcing of late Cenozoic climate. Nature 359:117–122

Rea DK, Snoeckx H, Joseph LH (1998) Late Cenozoic eolian deposition in the North Pacific: Asian drying, Tibetan uplift, and cooling of the northern hemisphere. Paleoceanography 13:215–224

Rieser AB, Liu Y, Genser J, Neubauer F, Handler R, Friedl G, Ge X-H (2006) 40Ar/39Ar ages of detrital white mica constrain the Cenozoic development of the intracontinental Qaidam Basin, China. Geol Soc Am Bull 118:1522–1534

Robinson DM, Dupont-Nivet G, Gehrels GE, Zhang YQ (2003) The Tula uplift, northwestern China: evidence for regional tectonism of the northern Tibetan Plateau during late Mesozoic-early Cenozoic time. Geol Soc Am Bull 115:35–47

Sepehr M, Cosgrove JW (2004) Structural framework of the Zagros Fold-Thrust Belt, Iran Marine and Petroleum. Geology 21:829–843

Shackleton NJ et al (1984) Oxygen isotope calibration of the onset of ice-rafting and history of glaciation in the North-Atlantic Region. Nature 307:620–623

Shen F, Royden LH, Burchfiel BC (2001) Large-scale crustal deformation of the Tibetan Plateau. J Geophys Res-Sol Ea 106:6793–6816

Song TG, Wang XP (1993) Structural styles and stratigraphic patterns of syndepositional faults in a contractional setting—Examples from Quaidam Basin, Northwestern China. Aapg Bull 77:102–117

Soofi MA, King SD (2002) Oblique convergence between India and Eurasia. J Geophys Res-Sol Ea 107: ETG 3-1-ETG 3-8

Spurlin MS, Yin A, Horton BK, Zhou J, Wang J (2005) Structural evolution of the Yushu-Nangqian region and its relationship to syncollisional igneous activity east-central Tibet. Geol Soc Am Bull 117:1293–1317

Sun JM, Zhu RX, An ZS (2005a) Tectonic uplift in the northern Tibetan Plateau since 13.7 Ma ago inferred from molasse deposits along the Altyn Tagh Fault. Earth Planet Sci Lett 235:641–653

Sun ZM et al (2005b) Magnetostratigraphy of Paleogene sediments from northern Qaidam Basin, China: implications for tectonic uplift and block rotation in northern Tibetan plateau. Earth Planet Sci Lett 237:635–646

Sun Z, Jing M, Sun N, Lu Y, Cao L (2007) Discussion on boundary between the upper and lower members of Xiaganchaigou Formation of Paleogene in Well Kun-2, Qaidam Basin. J Palaeogeogr 9:611–618

Tapponnier P, Peltzer G, Armijo R (1986) On the mechanics of the collision between India and Asia. Geol Soc Lond Spec Publ 19:113–157

Tapponnier P, Zhiqin X, Roger F, Meyer B, Arnaud N, Wittlinger G, Jingsui Y (2001) Oblique stepwise rise and growth of the Tibet plateau. Science 294:1671–1677

Thadani SG, Alabert F, Journel AG (1987) An integrated geostatistical/pattern recognition technique for characterization of reservoir spatial variability. Society of Exploration Geophysicists, New Orleans

Thomas WA (2001) Mushwad: ductile duplex in the Appalachian thrust belt in Alabama. Aapg Bulletin 85:1847–1869

Wan J, Wang Y, Li Q, Wang F, Wang EQ (2001) FT evidence of Northern Altyn uplift in late-Cenozoic Bulletin of Mineralogy. Petrol Geochem 20:222–224

Wang E (1997) Displacement and timing along the northern strand of the Altyn Tagh fault zone, northern Tibet. Earth Planet Sci Lett 150:55–64

Wang E (2004) An important form of basin-mountain coupling: orogenic belt and flank basin. Chin Sci Bull 49:632–636

Wang E, Xu FY, Zhou JX, Wan JL, Burchfiel BC (2006) Eastward migration of the Qaidam basin and its implications for Cenozoic evolution of the Altyn Tagh fault and associated river systems. Geol Soc Am Bull 118:349–365

Wang C et al (2008) Constraints on the early uplift history of the Tibetan Plateau. Proc Natl Acad Sci USA 105:4987–4992

Wang YD, Nie JS, Zhang T, Sun GQ, Yang X, Liu YH, Liu XW (2010) Cenozoic tectonic evolution in the western Qaidam Basin inferred from subsurface data. Geosci J 14:335–344

Wang CS et al (2011a) A mid-crustal strain-transfer model for continental deformation: a new perspective from high-resolution deep seismic-reflection profiling across NE Tibet. Earth Planet Sci Lett 306:279–288

Wang YD, Zhang T, Chi YP, Liu YR, Zhang ZG, Li SY, Fang XM, Zhang YZ (2011b) Cenozoic uplift of the Tibetan Plateau: evidence from tectonic-sedimentary evolution of the Western Qaidam Basin. Earth Sci Front 18:141–150 **(in Chinese with English abstract)**

Wang E et al (2012) Two-phase growth of high topography in eastern Tibet during the Cenozoic. Nat Geosci 5:640–645

Wang CS et al (2014) Outward-growth of the Tibetan Plateau during the Cenozoic: a review. Tectonophysics 621:1–43

Wesson R, Helley E, Lajoie K, Wentworth C (1975) Faults and future earthquakes Studies for seismic zonation of the San Francisco Bay region. US Geol Surv Prof Pap 941:A5–A30

Wu FY, Huang BC, Ye K, Fang AM (2008) Collapsed Himalayan: Tibetan orogen and the rising Tibetan Plateau. Acta Petrologica Sinica 24:1–30

Wu L, Xiao AC, Wang LQ, Mao LG, Wang L, Dong YP, Xu B (2012a) EW-trending uplifts along the southern side of the central segment of the Altyn Tagh Fault, NW China: insight into the rising mechanism of the Altyn Mountain during the Cenozoic. Sci China Earth 55:926–939

Wu L et al (2012b) Two-stage evolution of the Altyn Tagh Fault during the Cenozoic: new insight from provenance analysis of a geological section in NW Qaidam Basin, NW China. Terra Nova 24:387–395

Wu L, Xiao AC, Ma DD, Li HG, Xu B, Shen Y, Mao LG (2014) Cenozoic fault systems in southwest Qaidam Basin, northeastern Tibetan Plateau: geometry, temporal development, and significance for hydrocarbon accumulation. Aapg Bulletin 98:1213–1234

Xiao AC, Li JY, Zhang GS (1998) Structure and Kinematic Genesis of the Selibuya Strike-slip Duplex in the Tarim Basin. J JiangHan Petrol Inst 20:6–12 **(in Chinese with English abstract)**

Xie XA, Hu SY, Lu HF (1998) Positive inversion structure in the Bachu Fault-Uplift in the Tarim Basin. Geol Rev 44:1–6 **(in Chinese with English abstract)**

Yang CL (1999) Compressive-torsional structure system and hydrocarbon accumulation in the Tarim basin. Oil Geophys Prospect 34:682–689 **(in Chinese with English abstract)**

Yang MH, Jin ZJ, Lv XX, Pan WQ, Hu JF (2007) Basement-involved transpressional structure and the formation of the Bachu Uplift, Tarim Basin, Northwestern China. Acta Geol Sinica 81:158–165 **(in Chinese with English abstract)**

Yin A, Harrison TM (2000) Geologic evolution of the Himalayan-Tibetan orogen. Annu Rev Earth Planet Sci 28:211–280

Yin A, Harrison TM, Ryerson FJ, Chen WJ, Kidd WSF, Copeland P (1994) Tertiary structural evolution of the Gangdese thrust system, southeastern Tibet. J Geophys Res-Sol Ea 99:18175–18201

Yin A et al (2002) Tectonic history of the Altyn Tagh fault system in northern Tibet inferred from Cenozoic sedimentation. Geol Soc Am Bull 114:1257–1295

Yin A, Dang Y, Zhang M, McRivette MW, Burgess WP, Chen X (2007) Cenozoic tectonic evolution of Qaidam basin and its surrounding regions (part 2): wedge tectonics in southern Qaidam basin and the Eastern Kunlun Range. Geol Soc Am Spec Pap 433:369–390

Yin A et al (2008a) Cenozoic tectonic evolution of Qaidam basin and its surrounding regions (Part 1): the southern Qilian Shan-Nan Shan thrust belt and northern Qaidam basin. Geol Soc Am Bull 120:813–846

Yin A, Dang YQ, Zhang M, Chen XH, McRivette MW (2008b) Cenozoic tectonic evolution of the Qaidam basin and its surrounding regions (Part 3): structural geology, sedimentation, and regional tectonic reconstruction. Geol Soc Am Bull 120:847–876

Yin A, Dubey CS, Webb AAG, Kelty TK, Grove M, Gehrels GE, Burgess WP (2010) Geologic correlation of the Himalayan orogen and Indian craton: part 1. Structural geology, U-Pb zircon geochronology, and tectonic evolution of the Shillong Plateau and its neighboring regions in NE India. Geol Soc Am Bull 122:336–359

Yu XJ et al (2014) Anisotropy of magnetic susceptibility of Eocene and Miocene sediments in the Qaidam Basin, Northwest China: implication for Cenozoic tectonic transition and depocenter migration. Geochem Geophy Geosy 15:2095–2108

Yue YJ, Liou JG (1999) Two-stage evolution model for the Altyn Tagh fault, China. Geology 27:227–230

Yue YJ, Ritts BD, Graham SA (2001) Initiation and long-term slip history of the Altyn Tagh fault. Int Geol Rev 43:1087–1093

Zeng H (2013) Stratal slice: the next generation. Lead Edge 32:140–144

Zhang J (2007) A review on the extensional structures in the northern Himalaya and southern Tibet. Geol Bull China 26:639–649

Zhang PZ, Shen Z, Wang M, Gan WJ, Burgmann R, Molnar P (2004) Continuous deformation of the Tibetan Plateau from global positioning system data. Geology 32:809–812

Zheng DW et al (2006) Rapid exhumation at similar to 8 Ma on the Liupan Shan thrust fault from apatite fission-track thermochronology: implications for growth of the northeastern Tibetan Plateau margin. Earth Planet Sci Lett 248:198–208

Zheng DW, Clark MK, Zhang PZ, Zheng WJ, Farley KA (2010) Erosion, fault initiation and topographic growth of the North Qilian Shan (northern Tibetan Plateau). Geosphere 6:937–941

Zhisheng A, Kutzbach JE, Prell WL, Porter SC (2001) Evolution of Asian monsoons and phased uplift of the Himalaya-Tibetan plateau since Late Miocene times. Nature 411:62–66

Zhou JX, Xu FY, Wang TC, Cao AF, Yin CM (2006) Cenozoic deformation history of the Qaidam Basin, NW China: results from cross-section restoration and implications for Qinghai-Tibet Plateau tectonics. Earth Planet Sci Lett 243:195–210

Zhu LD, Wang CS, Zheng HB, Xiang F, Yi HS, Liu DZ (2006) Tectonic and sedimentary evolution of basins in the northeast of Qinghai-Tibet Plateau and their implication for the northward growth of the plateau. Palaeogeogr Palaeocl 241:49–60